Journal of the European Ceramic Society **15** (1995) 643–650

0955-2219(95)00030-5
0955-2219/95/$9.50

Creep Crack Growth in Alumina with a Glassy Phase

G. Martin, T. Fett & D. Munz

Forschungszentrum Karlsruhe, Institut für Materialforschung II and Universität Karlsruhe, Institut für Zuverlässigkeit und Schadenskunde im Maschinenbau, Karlsruhe, Germany

(Received 22 September 1994; revised version received 19 January 1995; accepted 31 January 1995)

Abstract

Creep-induced crack growth can be described with the C-integral as the relevant load parameter. Several possibilities of evaluating the C*-integral in single specimen tests are discussed, and the constant load and the constant loading-rate are applied to an alumina ceramic containing a glassy phase. The crack-growth rate as a function of the C*-integral is described by a power-law relation with an exponent which agrees very well with the theoretical value.*

1 Introduction

Fracture at elevated temperatures may be caused by subcritical crack propagation, which starts from existing flaws or from creep-induced damage caused by the formation and coalescence of pores. Whereas in the range of subcritical crack growth, which can be described by linear–elastic fracture mechanics, the stress intensity factor is the stress variable at the crack, this is the C^*-integral in the range of noticeable creep.[1] Creep-induced crack growth has very often been studied for metals, but investigations into ceramic materials are sparse.[2–4] It is the aim of this investigation to determine the crack-growth rates as a function of the C^*-integral for macroscopic cracks.

The C^*-integral — proposed by Landes and Begley[1] — is a path-independent energy-rate line integral. In the two-dimensional case (see Fig. 1) it is defined as

$$C^* = \int_\Gamma W^* \mathrm{d}y - T_i \frac{\partial v_i}{\partial x} ds \tag{1}$$

$$W^* = \int_0^{\epsilon_{ij}} \sigma_{ij} \mathrm{d}\epsilon_{ij} \tag{2}$$

where W^* is the strain-energy density rate, T_i is the traction vector, v_i is the displacement vector, and ds is a line length increment along the contour Γ.

The C^*-integral governs the stresses and strains in front of a crack tip. A premise for the applicability of the C^*-integral as a loading parameter is the occurrence of secondary creep, which may be described by a Norton power law

$$\dot{\epsilon}_s = D\,\sigma^n \tag{3}$$

Under this condition, an HRR-stress field occurs ahead of the crack tip.[5,6] The stresses and strain rates are given by

$$\sigma_{ij} = \left(\frac{C^*}{I_n D r}\right)^{\frac{1}{n+1}} \tilde{\sigma}_{ij}(\theta) \tag{4}$$

$$\dot{\epsilon}_{ij} = \left(\frac{C^*}{I_n D r}\right)^{\frac{n}{n+1}} \tilde{\sigma}_{ij}(\theta) \tag{5}$$

where $\dot{\epsilon}$ is the strain rate and $I_n(n)$ and $\tilde{\sigma}_{ij}(\theta)$ are the dimensionless functions, which can be taken from Ref. 6.

Under creep conditions, the application of a load instantly yields an elastic strain reaction. This elastic strain is superposed by creep strains. In the vicinity of the crack tip eqn (5) is immediately valid, but under non-steady-state creep conditions the parameter C^* has to be replaced by the time-dependent parameter $C(t)$.[7]

For very short times after load application, the stress intensity factor K is the relevant loading parameter, which describes the stresses at the crack tip

$$\sigma_{ij} = \left[\frac{\alpha K_I^2}{I_n D r (n+1)\, tE'}\right]^{\frac{1}{n+1}} \tilde{\sigma}_{ij}(\theta) \tag{6}$$

where $E' = E/(1-\nu^2)$ (E = Young's modulus, ν = Poisson's ratio). The numerical factor α is given in Ref. 7 as $\alpha \simeq 1$. With increasing size of the creep zone, the stress field is firstly governed by $C(t)$ and tends asymptotically to the C^*-controlled state. Since

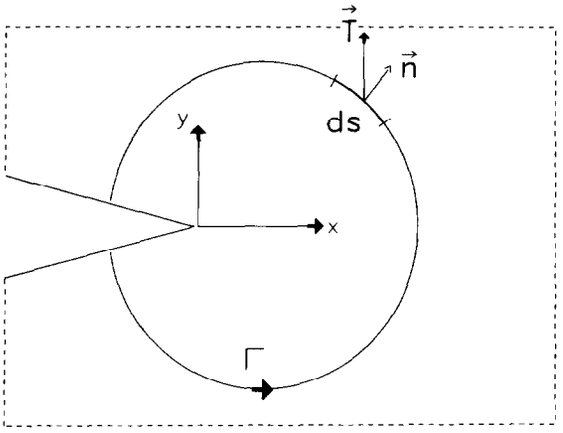

Fig. 1. Definition of the C^*-integral.

$$C(t) \to \frac{\alpha K_1^2}{(n+1)\, t\, E'} \text{ for } t \to 0 \tag{7}$$

and

$$C(t) \to C^* \text{ for } t \to \infty \tag{8}$$

Riedel[7] proposed the interpolation formula:

$$C(t) = \left(1 + \frac{t_1}{t}\right) C^* \tag{9}$$

for the region $t \simeq t_1$ with the characteristic time

$$t_1 = \frac{K_1^2}{(n+1)\, E' C^*} \tag{10}$$

In cases where primary creep dominates an additional integral quantity denoted C_h^* has to be applied. In this investigation we restrict our considerations to C^*.

2 The Experimental Determination of C^*

C^* can be expressed by the power difference of two identically loaded structures containing cracks of depths a and $a + da$, respectively, i.e.

$$C^* = -\frac{1}{B}\frac{dU^*}{da}, \quad U^* = \int_0^{\dot\delta} F\, d\dot\delta \tag{11}$$

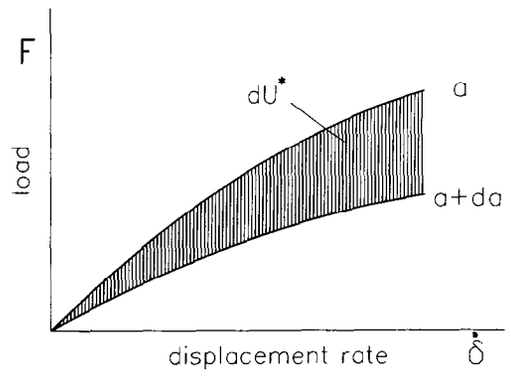

Fig. 2. Increment of energy rate dU^* for two cracks with crack lengths a and $a + da$.

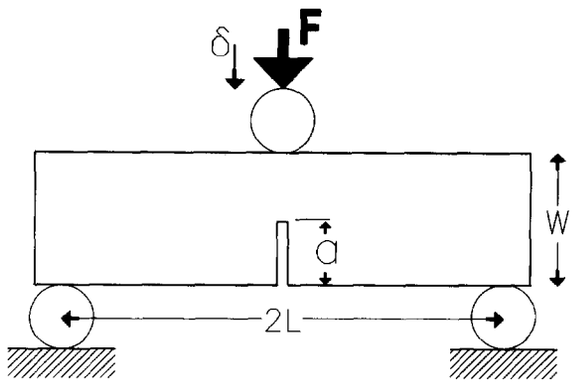

Fig. 3. Geometrical and loading quantities.

(B = specimen thickness). This relationship offers the possibility to determine C^* experimentally. The quantities entering eqn (11) are explained by Fig. 2. Equation (11) is the basis for a number of procedures for determination of C^*. The experimental data necessary for the evaluation of eqn (11) are the force F, the displacement rates $\dot\delta$ of the load application points, and the crack length a.

2.1 Single-specimen evaluation

The application of C^* as the crack-tip parameter was proposed by Landes and Begley[1] in analogy to the J-integral, the loading parameter in case of plastic material behaviour. J-integral solutions are available for numerous types of specimen and loading. In the EPRI-handbook[8] a number of FE-solutions are reported. Due to the analogy between Norton-like creep and strain-hardening plasticity,[9] the data of the EPRI-handbook can be used also for the computation of C^*. By introducing the net stress

$$\sigma_{\text{net}} = \frac{F}{B(W-a)} \tag{12}$$

Riedel[7] proposed the simple relation

$$C^* = aD\sigma_{\text{net}}^{n+1}\, g_1 \tag{13}$$

It should be noted that eqn (13) is only valid if the creep behaviour is correctly described by a Norton-relation. The geometric function $g_1(a/W,n)$ depends on the stress state and differs for plane-stress and plane-strain conditions. A second possibility to determine C^* — also proposed by Riedel[7] — is based on the measurement of the displacement rate at the load-application points

$$C^* = \sigma_{\text{net}}\, \dot\delta\, g_2 \tag{14}$$

with g_2 dependent on a/W and n. Based on the formulation eqn (11), Webster[10] derived

$$C^* = \frac{F^{n+1}}{B(n+1)}\frac{dC_n}{da} \tag{15}$$

with the creep-compliance

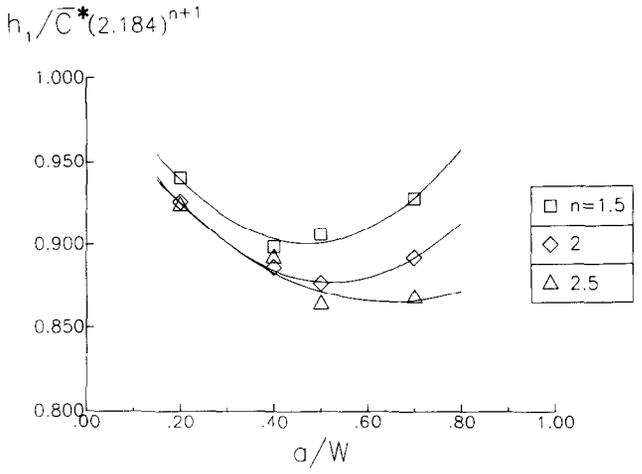

Fig. 4. Ratio of geometric functions from Walz[13] and the EPRI-handbook.[8]

$$C_n = \frac{\dot{\delta}}{F^n} \tag{16}$$

For a static test it results

$$C^* = \frac{F\dot{\delta}}{BW}\left[\frac{W}{n+1}\,\frac{1}{\dot{\delta}}\,\frac{d\dot{\delta}}{da}\right] \tag{17}$$

and in the dynamic loading case with constant displacement rates at the load application points

$$C^* = \frac{F\dot{\delta}}{BW}\left[-\frac{n}{n+1}\,\frac{W}{F}\,\frac{dF}{da}\right] \tag{18}$$

Based on the integral formulation of C^*, Harper and Ellison[11] derived for the static test (F = constant)

$$U^* = \frac{1}{n+1} DL \left(\frac{F}{m_{pl}BW}\right)^n F \tag{19}$$

and in case of constant displacement rates

$$U^* = \frac{n}{n+1} DL \left(\frac{F}{m_{pl}BW}\right)^n F \tag{20}$$

where L is the specimen length, for example the supported length of a bending bar and F is the applied load. m_{pl} is the ratio of the loads necessary to plastify the specimen with and without crack for ideal plastic material behaviour. Consequently, C^* results

$$C^* = -\frac{n}{n+1} DL \left(\frac{F}{m_{pl}BW}\right)^{n+1} \frac{dm_{pl}}{d(a/W)} \tag{21}$$

2.2 Multiple-specimen evaluation

The procedure of Landes and Begley comprises several steps. The detailed description is given in the original paper.[1]

(1) In the first step the load F is plotted as a function of the crack length a and the displacement rate $\dot{\delta}$. The area below the resulting curves gives the energy rate $U^*(a,\dot{\delta})$.

(2) The representation $U^* = f(\dot{\delta}, a)$ provides the derivative $\partial U^*/\partial a$ as a function of $\dot{\delta}$.

(3) From eqn (9) C^* is calculated and plotted versus $\dot{\delta}$.

(4) The basic data directly give $da/dt = f(a, \dot{\delta})$ and, finally, the combination of steps 3 and 4 results in the da/dt versus C^* curve.

This procedure has been applied successfully to Al_2O_3 which contains a glassy phase.[2,4] A further possibility to determine C^* has been proposed by Kanninen and Popelar.[12] Their procedure is based on tests with constant load where the crack length is determined as a function of time. The further procedure is identical with the evaluation according to the procedure proposed by Landes and Begley.[1]

In the present investigation the evaluation of single tests will be applied.

3 Determination of C^* in 3-point bending tests

The procedure of Landes and Begley, Kanninen and Popelar, Harper and Ellison and Webster are directly applicable in 3-point bending. With the relationships proposed in Ref. 7 also the J-integral solutions for bending tests can be used for the determination of C^*. The geometric functions g_1 and g_2 can be written in terms of the h-parameters h_1 h_2 tabulated in:[8]

$$g_{1b} = \left(\frac{W}{a} - 1\right) h_1 \left(\frac{L}{0{\cdot}728\,(W-a)}\right)^{n+1} \tag{22}$$

$$g_{2b} = \frac{h_1}{h_3}\,\frac{L}{0{\cdot}728a} \tag{23}$$

where the subscript b stands for bending. The geometric quantities L, a and W can be seen from Fig. 3. The C^*-integral can also be computed from

$$C^* = D(W-a)\, h_1 \left(\frac{FL}{0{\cdot}728B(W-a)^2}\right)^{n+1} \tag{24}$$

The h-parameters of the EPRI-handbook may be expressed by the following approximations for the range $2 \le n \le 7$

$$h_1 \simeq \alpha \left[1{\cdot}26 + \sum_{\nu=1}^{4}\sum_{\mu=1}^{3} A_{\nu\mu}\,(1-\alpha)^\nu n^{\mu/5}\right]^2 \tag{25}$$

$$h_3 \simeq \frac{1}{\alpha}\left[\sum_{\nu=0}^{3}\sum_{\mu=0}^{2} A_{\nu\mu}\,(1-\alpha)^\nu n^\mu\right]^2 \tag{26}$$

with $\alpha = a/W$ and the coefficients $A_{\nu\mu}$ listed in Table 1 for h_1 and in Table 2 for h_3

It is a well-known fact that ceramics containing a glassy phase exhibit non-symmetry in their creep behaviour. The creep rates under tensile stresses may be substantially higher than under compressive

Table 1. h-parameters. Coefficients for eqn (25)[4]

	$\mu = 1$	2	3
$\nu = 1$	4·4451	−4·552	0·1232
2	8·9083	−9·312	3·9838
3	−23·27	20·225	−3·790
4	13·543	−6·597	−1·333

Table 2. h-parameters. Coefficients for eqn (26)

	$\mu = 0$	1	2
$\nu = 0$	2·1204	−0·196	0·0153
1	−0·809	−0·287	−0·025
2	0·2307	0·7110	0·0519
3	0·4596	−0·326	−0·046

stresses. This behaviour affects heavily the bending creep test in which tension and compression occur. Very often, the non-symmetry is related only to the state of secondary creep. This seems to be the case e.g. for MgO-doped hot-pressed silicon nitride (HPSN).[14] If we take into consideration this non-symmetry, the Norton power law may be modified as

$$\dot{\epsilon}_s = \lambda\, D|\sigma|^n \tag{27}$$

with

$$\lambda = \left\{ \begin{array}{l} 1 \text{ for } \sigma > 0 \\ \dfrac{-1}{\gamma^n} \text{ for } \sigma < 0 \end{array} \right\} \tag{28}$$

and $\gamma > 0$.

In a Finite-Element study Walz[13] determined the C^*-integral in 3 point bending for a number of n-values and γ = 1, 5 and 10. The results are expressed by a geometric function C^* defined as

$$C^* = DW(1 - a/W)^{-(2n+1)}\bar{C}^*\,\sigma^{n+1} \tag{29}$$

where σ is the elastically calculated outer fibre bending stress. In case of symmetric creep behaviour (γ = 1), the geometric functions obtained by Walz[13] can be compared with the C^*-values according to eqn (24). From eqn (24) and eqn (29) one obtains

$$\bar{C}^* = \frac{h_1}{2{\cdot}184^{n+1}} \tag{30}$$

Figure 4 illustrates the quantity $h_1/\bar{C}^*2{\cdot}184^{n+1}$ as a function of α for several n-values. The deviations from the expected value 1 are caused by different values chosen for L/W. Whilst in the EPRI-handbook[8] L/W = 2 is used, the calculations of Walz[13] were performed with L/W = 4·4, as usual for ceramic bending bars. From the computations of Walz the geometric functions C^* were obtained, as listed in Tables 3 and 4.

4 Experiments

4.1 Material and measurements

The tested material was an Al_2O_3 containing a glassy phase. Short characterisation of the material used: density 3·75 g/cm^3, mean grain size 5 μm, composition 96% Al_2O_3 (2·7% SiO_2, 1·3% MgO, 0·02% CaO, 0·02% Fe_2O_3), fracture toughness 20°C: 3·4 MPa $\sqrt{m}$, 1100°C: 4·1–5·2 MPa $\sqrt{m}$, 1200°C: 3·1–5·0 MPa $\sqrt{m}$, elasticity data at 20°C E = 325 GPa, ν = 0·24. In 4-point bending creep tests the parameters of secondary creep were determined as:[4] n = 2·25, $D = 1{\cdot}4 \times 10^{-8}$ (in MPa, h), γ = 5·1. Bending specimens, 3·5 × 4·5 × 45 mm in size, were diamond machined and then annealed in the vacuum for 5 h at 900°C. Then the specimens were damaged by introducing narrow saw cuts of 50 μm width. A second series of bending bars was precracked using the bridge indentation method. The static and dynamic tests were performed in a testing device as used in creep tests.[14] With this device the displacements can be measured within the inner roller span where the bending moment is constant. The 3-point bending tests were carried out with a modified device where the outer displacement pick-ups were applied directly under the outer rollers. All bending tests were performed with $2L$ = 40 mm. The experimental input for the determination of C^*

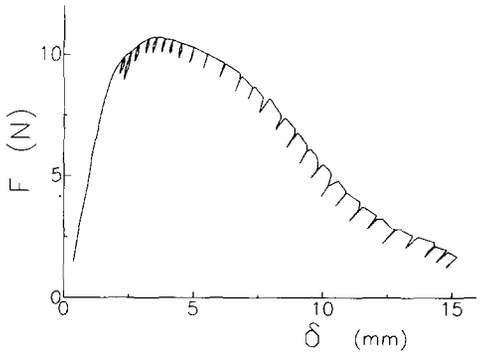

Fig. 5. Partial unloadings in a dynamic bending test.

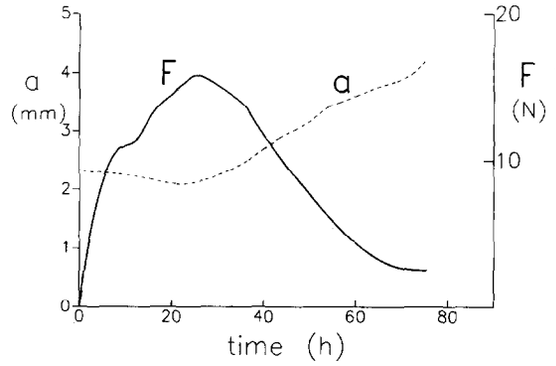

Fig. 6. Dynamic bending test (displacement rate: 2 μm/h).

Table 3. Geometric function $\overline{C}^*$ according to eqn (29) for $\gamma = 5$

a/W	$n = 1{\cdot}5$	2	2·5
0·1	0·0470	0·0242	0·0127
0·2	0·0644	0·0335	0·0163
0·3	0·0664	0·0344	0·0144
0·4	0·0621	0·0314	0·0107
0·5	0·0577	0·0275	0·0077
0·6	0·0553	0·0241	0·0068
0·7	0·0541	0·0215	0·0084
0·8	0·0495	0·0183	0·0120

Table 4. Geometric function $\overline{C}^*$ according to eqn (29) for $\gamma = 10$.

a/W	$n = 1{\cdot}5$	2	2·5
0·1	0·0393	0·0163	0·0065
0·2	0·0577	0·0153	0·0061
0·3	0·0586	0·0109	0·0045
0·4	0·0503	0·0091	0·0030
0·5	0·0403	0·0104	0·0026
0·6	0·0356	0·0126	0·0032
0·7	0·0424	0·0151	0·0043
0·8	0·0662	0·0215	0·0044

are the load–displacement curves and the crack-length data which are determined from partial unloadings. During the periodical partial unloadings the displacements are recorded. An example is shown in Fig. 5. The slopes of the partial unloadings decrease with increasing crack length. During partial unloading and reloading hysteresis effects were observed. Therefore, the usually applied linear–elastic compliance relationship could not be applied. Dynamic bending tests were interrupted in different states and the specimens were broken at room temperature. Then it was possible to measure the crack size on the fracture surface, and one point of the relationship slope of the hysteresis = $f(a)$ has been determined. A series of such tests then yielded the complete calibration curve. The result of a single cynamic bending test performed with a bar containing a saw-cut of 50 μm width and $a/W \simeq 0{\cdot}5$, with a displacement rate $\dot{\delta} = 2$ μm/h, is shown in Fig. 6. The crack starts propagating approximately when the maximum load is reached, and the following crack growth is nearly proportional to the time.

4.2 Evaluation of constant load tests

The loading-point displacements occurring in a creep-crack-growth test consist of three contributions:

- the creep deformations δ_c caused by the singular stress field close to the crack tip;
- the share of global creep deformation occurring in the remote parts of the specimen, δ_{nc}, and
- the contribution caused by an increase in compliance due to crack extension δ_{el}.

The measurable total displacements are

$$\delta_{meas} = \delta_c + \delta_{nc} + \delta_{el} \tag{31}$$

Due to the change of crack length during creep crack growth, an elastical displacement rate $\dot{\delta}_{el}$ occurs. In order to consider only creep effects, the elastic part has to be eliminated, i.e.

$$\dot{\delta} = \dot{\delta}_{meas} - \dot{\delta}_{el}, \quad \dot{\delta}_{el} = F \frac{\partial C}{\partial a} \dot{a} + C\dot{F} \tag{32}$$

or it has to be ensured that the elastic part can be neglected. Displacement rates obtained in a constant load test are plotted in Fig. 7. Whereas the total displacement rate $\dot{\delta}_{meas}$ was experimentally determined, the quantity $\dot{\delta}_{nc}$ was measured in a separate test with an unnotched specimen and $\dot{\delta}_{el}$ was computed from the time-dependent increase in crack length.

As a premise for the correct determination of dU^*/da it has to be ensured that crack propagation had taken place and that the minimum displacement rate in a test has been reached. In Fig. 8 the crack-growth initiation times — the time span between the moment of load application and

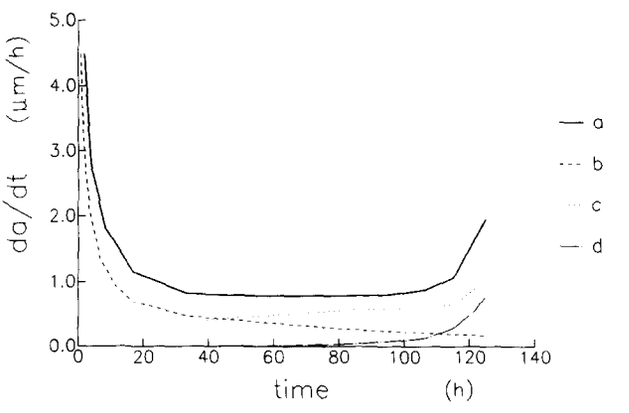

Fig. 7. Displacement rates in a constant load test.; (a) $\dot{\delta}_{meas}$; (b) $\dot{\delta}_{nc}$; (c) $\dot{\delta}_c$; (d) $\dot{\delta}_{el}$.

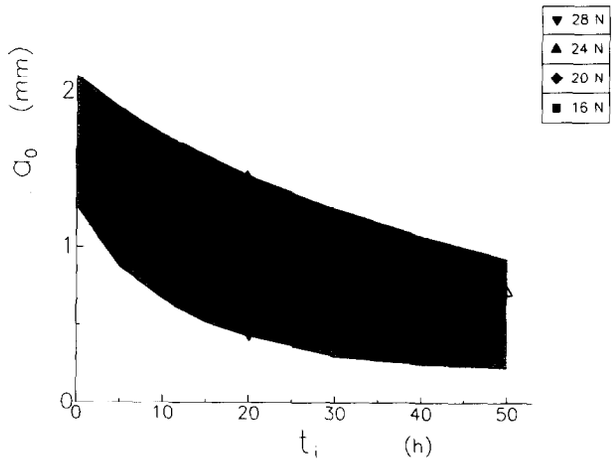

Fig. 8. Initiation times for creep crack growth tests under static load as a function of the initial crack length a_o; solid symbols: cracks introduced by a saw-cut of 50 μm width, open symbols: pre-cracked by the bridging method.

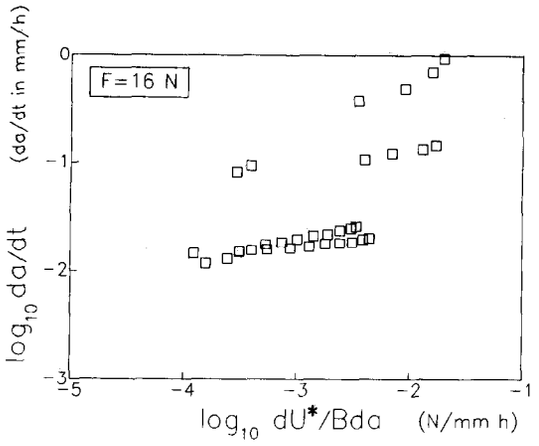

Fig. 9. Crack-growth rate as a function of dU^*/da.

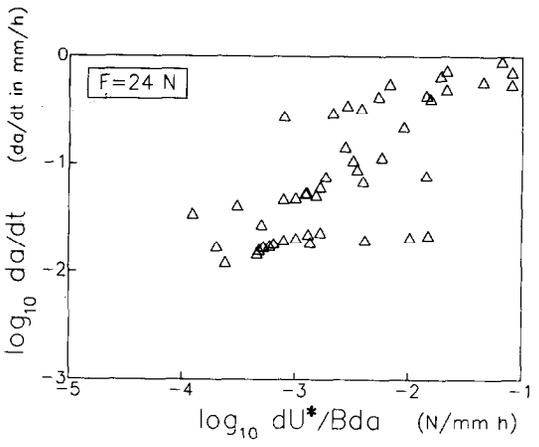

Fig. 11. Crack growth rate as a function of dU^*/da.

the first detectable crack extension — are plotted as a function of the initial crack length a_0.

It can be seen that no significant difference exists between specimens with saw-cut and with precrack. The tendency of decreasing crack-growth initiation time with increasing initial crack size is perceptable and has been expected.

Several series of static bending tests were evaluated with the method proposed by Webster,[10] eqn (17). The change of creep power with crack length was determined for test times $t > 20$ h at 8 h intervals and for times $t < 20$ h in time steps of 1–2 h until the specimens failed or the tests were suspended. All test durations were within 5 h and 340 h. The results are plotted in Figs 9–12.

4.3 Determination of C^*

The values dU^*/da determined in the experiments have to be examined out whether or not they represent valid C^*-values. In order to decide this, we have to compute the characteristic times t_1, using eqn (10). For times $t > 10\ t_1$ we expect the results to be valid C^*-values. Figure 13 shows the results of the constant load tests. The data undergo much scatter. There is some evidence that the very low crack-growth rates may be caused by R-curve effects. The R-curve behaviour shields the crack-tip region from the externally applied loads which results in lower crack-tip loading and, consequently, lower crack-growth rates. A clear indication is the reduction of the scatter band if only the first C^*-data of each test is considered. These data are introduced in Fig. 13 as solid symbols. For these tests the R-curve, for instance caused by crack-bridging effects, does not influence the result since $\Delta a = a - a_0 \to 0$. Fitting the solid symbols we find the power-law relation of creep-crack growth

$$\frac{da}{dt} = 6{\cdot}9\ \frac{\text{mm}}{\text{h}}\ C^{*0{\cdot}77} \tag{33}$$

(C^* in N/mm h). The corresponding straight line is entered in Fig. 13. Figure 14 shows the data resulting from times $t_1/10 \le t \le 10\ t_1$ evaluated according to eqn (9). These data can be expressed by

$$\frac{da}{dt} = 4{\cdot}4\ \frac{\text{mm}}{\text{h}}\ C(t)^{0{\cdot}71} \tag{34}$$

($C(t)$ in N/mm h). For identical crack-growth rates $C(t)$ is slightly lower than C^*. Riedel[7] has shown that the exponent of the creep-crack growth relation should be a simple function of the Norton creep exponent, namely

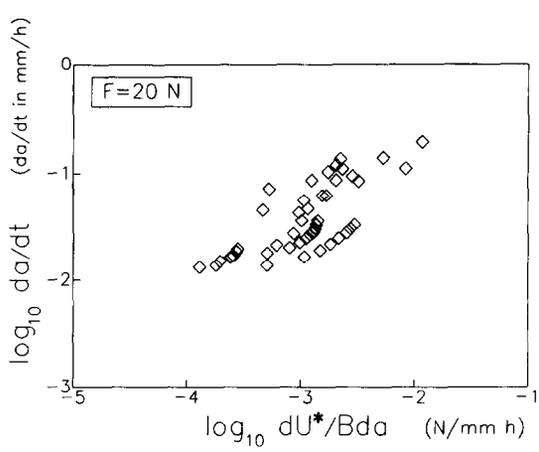

Fig. 10. Crack-growth rate as a function of dU^*/da.

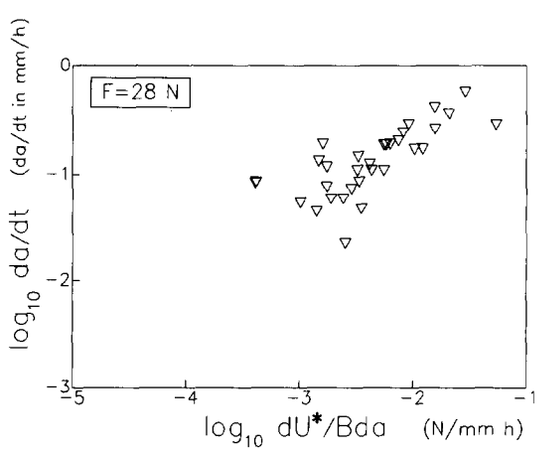

Fig. 12. Crack-growth rate as a function of dU^*/da.

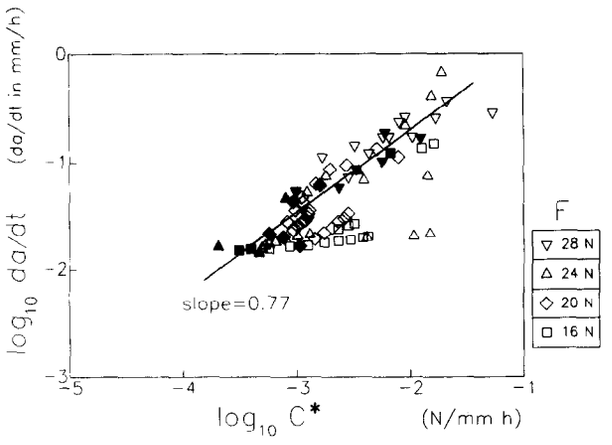

Fig. 13. Crack-growth rate as a function of C^* from static tests. Solid symbols: first values at the beginning of crack extension.

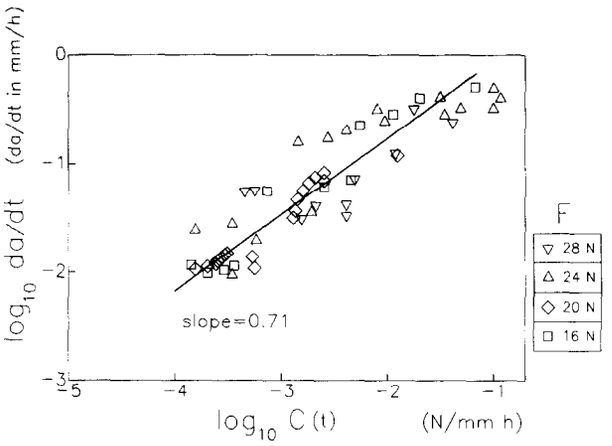

Fig. 14. Crack-growth rate as a function of $C(t)$ from static tests.

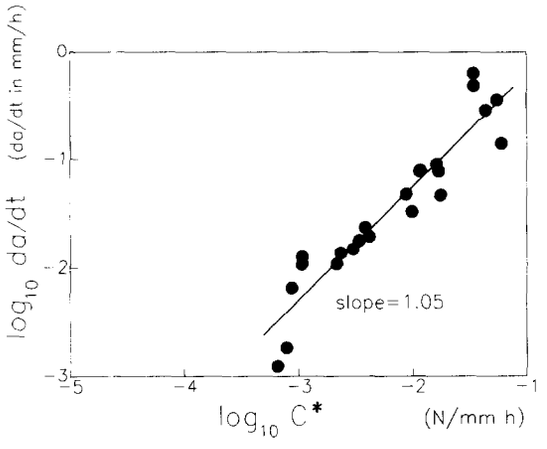

Fig. 15. Crack-growth rate as a function of C^* from dynamic tests.

$$\frac{da}{dt} \propto C^{*n/(n+1)} \tag{35}$$

leading for the investigated material ($n = 2{\cdot}25$) to an exponent of 0·69. This expected value is in very good agreement with the experimental result.

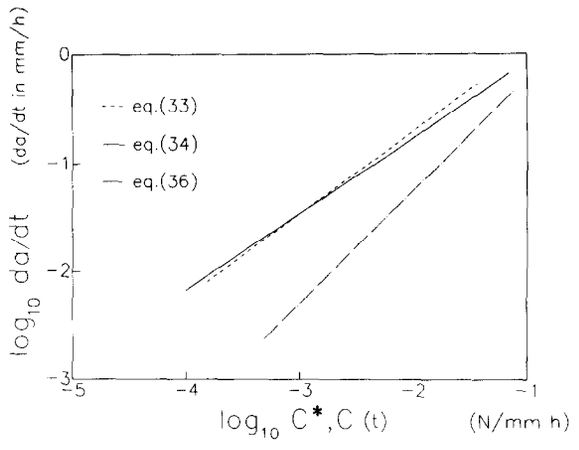

Fig. 16. Intercomparison of the crack-growth relations.

4.4 Evaluation of dynamic bending tests

The single-specimen evaluation from the dynamic tests (tests with constant displacement rates) was performed with eqn (18). It was assumed that in the range of decreasing load steady-state creep conditions are sufficiently fulfilled. The tests were performed with displacement rates in the range from 0·2 μm/h to 10 μm/h. The initial crack sizes were in the range 1 mm $\leq a_0 \leq$ 2·3 mm. In the region where the tests were evaluated the corresponding loads were between 8 and 22 N. Since, unfortunately, the crack-growth rates in the range of decreasing load were found to be highly constant in each test, it was only possible to determine one single C^*-value for one da/dt-value. Figure 15 shows the data obtained. Also in these tests a power law was found

$$\frac{da}{dt} = 6{\cdot}9 \ \frac{\text{mm}}{\text{h}} \ C^{*1{\cdot}05} \tag{36}$$

(C^* in N/mm h). The slightly increased exponent of 1·05 may be caused by R–curve influences. In case of the dynamic tests, the cracks had strongly grown by about 1·4 mm to attain the range of decreasing load. In the static tests the mean crack extension was only $\simeq$ 0·3 mm. Consequently, R–curve effects are stronger in the dynamic tests since $\Delta a \not\to 0$.

A comparison of the crack-growth relations, eqns (33), (34) and (36), is given in Fig. 16.

5 Summary

The paper deals with the determination of the loading quantities C^* and $C(t)$ for creep-crack growth. Different possibilities of evaluating the C^*-integral in single-specimen tests were listed, and the constant load test and the constant loading-rate test were applied to an alumina ceramic

containing a glassy phase. It was found that:

- the crack-growth rate as a function of the loading quantities C^* and $C(t)$ can be described by a power-law relationship;
- the exponents in static tests are about 0·75 and agree very well with the theoretical value (here: 0·69) proposed by Riedel;[7]
- the exponent resulting in tests with constant displacement rate is slightly higher, possibly influenced by R–curve effects.

References

1. Landes, J. D. & Begley, J. A., *ASTM STP 590*, 1976, pp. 128–48.
2. Kromp, K., Haug, T., Pabst, R. F. & Gerold, V., *C* for ceramic materials?, 3. Conf. on Creep and Fracture of Engineering Materials and Structures*, London, 1989, pp. 1021–32.
3. Martin, G., Fett, T. & Munz, D., *Determination of creep crack growth in ceramics*, Proc. 2nd ECRS-Conference, Augsburg, 1991.
4. Fett, T., Mißbach, M. & Munz, D., Failure behaviour of Al_2O_3 with glassy phase at high temperatures. *J. Europ. Ceram. Soc.*, **13** (1994) 197–209.
5. Hutchinson, J. W., Plastic stress and strain fields at crack tip. *J. of Mech. and Phys. of Solids*, **16** (1968) 13–31.
6. Rice, J. R. & Rosengren, G. F., Plane strain deformation near crack tip in power law hardening material, *J. of Mech. and Phys. of Solids*, **16** (1968) 1–12.
7. Riedel, H., *Fracture at high temperatures*, Springer-Verlag, Berlin, 1987.
8. Kumar, V., German, M. D. & Shih, C. F., An engineering approach for elastic–plastic failure analysis. *EPRI-Report NP-1931*, Palo Alto, 1981.
9. Hoff, N. J., Approximate analysis of structures in the presence of moderately large creep deformations *Quarterly of Applied Mathematics*, **12** (1954) 49–55.
10. Webster, G. A., *Crack growth at high temperatures*, Conference on Mechanics and Physics of Fracture, Paper 18. Cambridge, 1975.
11. Harper, M. P. & Ellison E. G., The use of the C^* parameter in predicting creep crack propagation rates. *J. of Strain Analysis*, **12** (1977).
12. Kanninen, M. F., Popelar, C. H., *Advanced Fracture Mechanics*, Oxford Engineering Science Series 15, Clarendon Press, Oxford, 1985 p. 437.
13. Walz, G., unpublished results.
14. Fett, T., Keller, K. & Munz, D., An analysis of the creep of hot-pressed silicon nitride in bending. *J. Mater. Sci.*, **23** (1988) 467–74.